Published in final edited form as:
IEEE Trans Neural Syst Rehabil Eng. 2011 February ; 19(1): 84–94. doi:10.1109/TNSRE.2010.2065241.

Effects of Biphasic Current Pulse Frequency, Amplitude, Duration and Interphase Gap on Eye Movement Responses to Prosthetic Electrical Stimulation of the Vestibular Nerve

Natan S. Davidovics, **Gene Y. Fridman[Member, IEEE]**, **Bryce Chiang**, and **Charles C. Della Santina[Member, IEEE]**
Depts of Otolaryngology Head and Neck Surgery and Biomedical Engineering, Johns Hopkins School of Medicine, 601 N. Caroline Street, Rm 6253, Baltimore, MD 21287, USA, phone 410-502-7909; fax 410-614-8610

Charles C. Della Santina: cds@jhmi.edu

Abstract

An implantable prosthesis that stimulates vestibular nerve branches to restore sensation of head rotation and vision-stabilizing reflexes could benefit individuals disabled by bilateral loss of vestibular (inner ear balance) function. We developed a prosthesis that partly restores normal function in animals by delivering pulse frequency modulated (PFM) biphasic current pulses via electrodes implanted in semicircular canals. Because the optimal stimulus encoding strategy is not yet known, we investigated effects of varying biphasic current pulse frequency, amplitude, duration and interphase gap on vestibulo-ocular reflex (VOR) eye movements in chinchillas. Increasing pulse frequency increased response amplitude while maintaining a relatively constant axis of rotation. Increasing pulse amplitude (range 0–325 μA) also increased response amplitude but spuriously shifted eye movement axis, probably due to current spread beyond the target nerve. Shorter pulse durations (range 28–340 μs) required less charge to elicit a given response amplitude and caused less axis shift than longer durations. Varying interphase gap (range 25–175 μs) had no significant effect. While specific values reported herein depend on microanatomy and electrode location in each case, we conclude that PFM with short duration biphasic pulses should form the foundation for further optimization of stimulus encoding strategies for vestibular prostheses intended to restore sensation of head rotation.

Index Terms

vestibular; neural; prosthesis; pulse duration; interphase gap; electrical stimulation; vestibular implant

I. Introduction

A. Background

Profound bilateral loss of vestibular sensation disables vestibulo-ocular and vestibulo-spinal reflexes that normally stabilize gaze and posture [1]. Affected individuals suffer oscillopsia (illusory movement of the visible world during head motion), postural instability and chronic disequilibrium [2–6]. Apart from vestibular rehabilitation exercises designed to augment deficient vestibular reflexes via central adaptation, there is no definitive treatment for individuals disabled by profound bilateral vestibular sensory loss.

Normally, both eyes rotate opposite the direction of head rotation in order to stabilize images on the retinae. This compensatory rotation is driven by the vestibulo-ocular reflex

(VOR), for which sensory input is provided by three mutually orthogonal semicircular canals (SCC) in each inner ear's vestibular labyrinth. Discharge rates of vestibular afferent fibers in each SCC's ampullary nerve are modulated by the component of head angular velocity about that SCC's axis [1,7–9]. Classic studies by Cohen, Suzuki and colleagues [10–13] revealed that selective electrical stimulation of a single ampullary nerve elicits extraocular muscle activation patterns that rotate both eyes about the axis of that SCC. Drawing on those results, Gong and Merfeld *et al.* designed the first prototype vestibular prosthesis intended to partially restore vestibular function in otherwise normal guinea pigs and squirrel monkeys rendered unresponsive to head rotation by surgical plugging of SCCs [14–20]. By delivering biphasic, symmetric, charge-balanced pulses at rates modulated by a single-axis head-mounted gyroscope in these animals, the device generated partly compensatory eye movements for head rotations about the gyro's axis of rotational sensitivity.

We extended this approach to a multichannel vestibular prosthesis capable of sensing and encoding 3-dimensional (3D) head rotation via stimulation of all three ampullary nerves in the labyrinth [21–24]. In those studies, we encountered several design trade-offs impacting the dynamic range over which the device accurately encodes both head velocity amplitude and axis. For example, increasing current amplitude of symmetric, charge-balanced, biphasic stimulus pulses resulted in higher VOR velocities but also increased misalignment between the desired and observed VOR axes of rotation [23]. Typically, we found prosthetic stimuli could evoke VOR responses up to ~50°/s peak velocity without incurring significant misalignment, but more intense stimuli incurred increasing misalignment between the axes of the eye movement response and the head rotation being encoded. Optimizing the tradeoff between dynamic range and axis misalignment of electrically-evoked VOR responses will be necessary if a vestibular prosthesis is to accurately encode 3D head rotations over the full range of natural head movements encountered in daily life, which often exceed 300 °/s in humans [25].

The focus of the present study is on design of stimulation protocols that optimize this tradeoff. While efforts continue toward improving performance along other design aspects, it is worth noting that much of the improvement in cochlear implant speech discrimination outcomes over the past 20 years has been due to changes in stimulus mapping protocols independent of changes in electrode design [26–28]. Optimization of stimulus timing has also yielded improved results in stimulation of peripheral motor nerve [29,30] and retinal ganglion cells [31].

B. Optimization of the Stimulus Parameters

Although the prosthesis circuitry used for the experiments described in this paper can generate arbitrarily shaped charge-balanced pulses [22,23], we have so far limited our studies to biphasic, symmetric, constant-current-per-phase pulses that are initially cathodic at the working (intralabyrinthine) electrode with respect to a larger distant electrode embedded either in the neck musculature or in the common crus (segment of labyrinth that is part of both the anterior and posterior SCCs) of the labyrinth. Charge balancing the cathodic and anodic phases is necessary to prevent irreversible corrosion of electrodes and deposit metal oxides at the electrode-tissue interface [32]. Pulse-frequency modulated, symmetric, constant-current-per-phase biphasic pulses are defined by four parameters [Fig. 1(A)]: pulse frequency, current amplitude, pulse duration (PD) for each phase of the pulse, and duration of the zero-current interphase gap (IPG) between opposite polarity pulse phases.

Single-unit recording studies from all vertebrate species tested so far suggest that most vestibular nerve afferent fibers in each SCC's ampullary nerve encode the component of head angular movement about that SCC's axis via modulation of action potential firing rate

by head angular velocity over the frequency range encompassing most head movements [33–35]. Accordingly, pulse frequency modulation by head velocity is probably the most appropriate basic scheme for encoding gyro inputs into physiologically meaningful electrode outputs for a vestibular prosthesis. In fact, all prior studies of head-mounted vestibular prostheses have used a variation of pulse-frequency modulation by head velocity [7,14–20,23,36,37].

Pulse duration can play an important role independent of the current amplitude and total charge injected by charge-balanced biphasic pulses, particularly for short PD [29,32]. Measurements of auditory brainstem response thresholds during cochlear nerve stimulation in guinea pigs [38] showed that doubling PD from 1 ms to 2 ms reduced the threshold current by an average of only 4.2 dB, instead of the expected 6 dB if the neural activation threshold were dependent only on the total charge of the stimulus pulse. In other words, pulses with shorter PD required less total charge to elicit a threshold response, consistent with classical strength-duration curve descriptions of action potential initiation and other threshold responses to sensory input [39–42]. In addition to influencing the amount of charge required to depolarize an axon, varying the PD may also affect spatial selectivity of exogenous current stimuli, as illustrated by both neuromorphic models and experimental data [29,31,43,44]. In the present study, we sought to determine whether this effect manifests in the setting of prosthetic vestibular nerve stimulation as an improvement of VOR axis alignment for shorter PD stimuli.

Multiple groups working with cochlear and motor nerves have reported that as the IPG of symmetric charge-balanced cathodic-first biphasic pulses decreases, a pulse pair becomes less efficient at activating the target nerve cell, so that greater current amplitude is required to exceed the response threshold [45–48]. For IPGs that are long compared to PD, the biphasic pulse becomes nearly as efficient as a non-charge-balanced monophasic pulse for eliciting threshold responses in cochlear nerve stimulation [47,49]. However, IPG variation seems to only exhibit a minor effect on loudness perception [46,48,50]. Furthermore, van Wieringen *et al.* [51] determined in a psychophysical cochlear implant study that there was no significant difference in the spatial selectivity (the region of neurons being activated) of the biphasic pulses for different IPG durations. Given the disparity between IPG effects on auditory nerve single fiber thresholds and psychophysical outcomes, and considering that the fundamental coding scheme used in prosthetic vestibular stimulation differs from that used in the cochlear implants (pulse frequency modulation as opposed to pulse amplitude modulation encoding the envelope of a signal), one cannot easily infer the effect of IPG variation on VOR responses from existing literature on IPG in cochlear implants. We therefore sought to characterize this dependence.

II. Materials and Methods

A. Surgery

Five adult wild-type 450–650 g chinchillas (*Chinchilla lanigera*) were used for all experiments. Surgical procedures were conducted in accordance with a protocol approved by the Johns Hopkins Animal Care and Use Committee and described in detail previously [23]. In summary, under general anesthesia a phenolic post was positioned in the midline perpendicular to the skull at the bregma and embedded in dental cement extruded into each bulla. The post served to restrain the animal during testing. Monopolar stimulating electrodes were inserted in each SCC of one labyrinth in each animal.

The electrode intended for anterior SCC ampullary nerve stimulation was positioned just medial of the anterior canal ampulla. The electrode intended for horizontal SCC ampullary nerve stimulation was inserted into the horizontal canal anterolateral of the horizontal

ampulla between the canal wall and the membranous labyrinth. The electrode intended for posterior SCC ampullary nerve stimulation was inserted toward the crista via a fenestration in the posterior canal. A "distant" reference electrode was implanted in neck musculature and a "near" reference electrode was positioned in the common crus. Whichever reference electrode elicited threshold VOR eye movements at the lowest current amplitude was chosen as the reference for all subsequent tests using that SCC electrode.

At the time of electrode implantation, all three SCCs of the contralateral labyrinth were plugged with fascia and bone chips to render that labyrinth insensitive to head rotation. The implanted SCCs were not plugged, so that effects of electrode implantation on SCC and cochlear function could be measured as part of a related study [52].

B. Measuring VOR Response

We used a real time, binocular 3 dimensional video-oculography (3D VOG) system modified slightly from one described previously in detail [53] for recording eye movements in response to electrical stimulation of the SCCs. In summary, an array of three fluorescent yellow squares on a black film was placed on the topically anesthetized cornea of each eye using a small amount of veterinary tissue glue (VetBond, 3M Corp) after application of proparacaine and saline eye drops. Firewire cameras (Dragonfly Express, Point Grey Research) retrofitted with 25 mm focal length, f/2.0 microvideo lenses were used to acquire 500 × 400 pixel images at 179 Hz for each eye using custom software in LabVIEW.

C. Stimulation paradigm

The essential scheme by which the Johns Hopkins Multichannel Vestibular Prosthesis version 1 (MVP1) encodes head rotational velocity about each of 3 SCC plane axes is by modulating the frequency of symmetric, charge-balanced, cathodic-first (at the SCC electrode), constant current pulses [23]. In order to ensure measured responses were due solely to prosthetic input, the head and body were kept stationary during measurements of the prosthetically-evoked VOR eye movements, and the MVP1's gyroscopic signals were replaced with analog signals representing 3 head rotation components delivered under computer control in a dark room by a USB-3103 DAQ card (Measurement Computing, Norton, MA). In order to selectively probe the response to stimulation targeting a single ampullary nerve, only one channel of the prosthesis was activated in any one set of experimental trials.

Before modulation began, animals were acclimated to a mean baseline pulse rate of 60 pulses per second (pps), which approximates the mean resting firing rate of normal vestibular afferents in chinchilla [33,54] and, therefore, allows for a dynamic range of stimulus modulation that is similar to normal. Animals were allowed to acclimate to this baseline stimulation until the frequency of "spontaneous" nystagmus quick phases had fallen to <1 per 30 sec of observation, suggesting the animal had adapted to the baseline stimulation. This typically took ~ 1–5 minutes. Whenever stimulation parameters were changed, we allowed sufficient time (typically <1 minute) to elapse for the animal to adapt by waiting until there was no visible nystagmus. Although all biphasic stimulus pulses were presumed to be excitatory in this setting, adapting the animal to a non-zero baseline stimulation rate allowed encoding of both excitatory and inhibitory head rotations by increasing or decreasing the pulse rate about the baseline [18,23].

The pulse rates on each electrode were encoded via a velocity-to-pulse-frequency mapping varying from 0 to 400 pps [Fig. 1(B)] designed to roughly approximate the firing pattern of vestibular nerve afferents [55, 56]. This mapping was piecewise linear on 2 segments, with inhibitory head rotations of 0 to −300°/s mapping to 0–60 pps and excitatory head rotations

of 0 to + 300°/s mapping to 60–400 pps. Thus, excitatory head rotations elicited an increased dynamic range (5.7X) and gain response than did inhibitory rotations of the same speed, as is the case in normal animals. For all experiments, the pulse frequency was modulated at 2 Hz to represent sinusoidal head movements at 2 Hz. This modulation frequency was chosen because it is within the range for which the VOR is important for gaze stabilization [23, 57].

The piecewise-linear relationship we used to relate head angular velocity to pulse frequency causes potential confusion when describing a given modulating stimulus, because, for example, a 100°/s amplitude sinusoidal head velocity vs. time waveform maps to an asymmetric modulation of pulse frequency in which the excitatory half cycles modulate up from 60–173 pps and the inhibitory half cycles modulate down from 60–40 pps. Moreover, our use of computer-controlled inputs to take the place of actual gyro signals precludes the use of actual head angular velocity as the input variable. We therefore report modulation of stimulation pulse frequency in terms of stimulus intensity (SI). An SI of 0% (representing no head movement) refers to stimulation at a constant 60 pps while an SI 100% (representing sinusoidal head movements of 300°/s peak, at the high end of velocities in typical head movements of normal chinchillas) refers to modulation of the pulse rate from 0 to 400 pps (with a baseline stimulation rate of 60 pps, as before).

Probably due to variation in electrode placement, different implanted SCCs yielded different peak VOR response velocities to a given SI. Analogous to programming a cochlear implant, each stimulating electrode of the vestibular prosthesis can be programmatically mapped to elicit the appropriate VOR gain when stimulated with a given SI by scaling the output voltage of the gyroscopes. For example, an electrode that evokes maximum eye movements of 200°/s in response to 100% SI might have a velocity-to-pulse-frequency mapping in which 400°/s peak head velocity would correspond to 400 pps and −400°/s to 0 pps, thereby eliciting a normal chinchilla VOR gain of ~0.5 [23,57]. In contrast, a chinchilla with maximum evoked eye movements of 400°/s in response to 100% SI might have a mapping in which 400°/s peak head velocity would correspond to 230 pps and −400°/s to 30 pps (50% SI) to achieve the same VOR gain of ~0.5.

D. Pulse-Frequency Modulation

We hypothesized that pulse-frequency modulation of constant-current, constant-charge/phase, biphasic pulse stimuli can encode a wide range of head velocities without significant change in the axis of VOR eye rotation (which presumably approximates the antisense of the perceived axis of head rotation). To test this hypothesis, we measured VOR eye movements in response to SI ranging from 0% to 100% in random order for 5 implanted SCCs. We delivered 2 Hz modulated pulse trains to the target electrode with PD = 340 μs and current amplitude equal to halfway between threshold and maximum delivered current (current at which facial twitching was first observed). All pulses were presented asynchronously to avoid overlap of current injection. Misalignment was defined as the minimum angle subtended in 3D space between the axis of observed eye rotations and the desired axis (the axis of the SCC being stimulated).

E. Pulse Duration and Current Amplitude

To explore the effects of varying current amplitude and PD in vestibular stimulation, we measured VOR eye movement responses to stimulation delivered independently via each electrode using various combinations of the two parameters, while keeping the IPG constant at 25 μs and using an SI of 100%. For each implanted electrode, nine different current amplitudes were paired with each one of the following PDs: 28, 50, 100, 180, 270, and 340 μs. The minimum current amplitude used was selected for each PD by steadily increasing

the current amplitude on the target electrode until a threshold periodic eye movement was observed. The maximum current amplitude was defined as that at which facial twitching was first observed, which is likely caused by unintended stimulation of the facial nerve (a branch of which courses near the SCC ampullae). Seven equally spaced current amplitudes were selected between the minimum and maximum to adequately sample the eye responses at different current amplitudes. Each combination of current amplitude and PD was then presented to the animal over ten repeated cycles. In order to examine effects solely due to changes in PD and current on the SCC under test, the current amplitude on the two non-modulating electrodes was set to 0. This process was repeated for the each implanted electrode for each animal. Misalignment was calculated for each PD at a constant eye velocity equal to half the maximum velocity observed for excitation of that SCC.

F. Interphase Gap Experiments

To understand how varying IPG influences VOR responses, we presented pulse trains with IPGs of 25, 50, 75, 100, 125, 150, and 175 μs, and PDs of 180 μs or 340 μs, at a constant current amplitude set to the middle of the range between threshold and maximal stimulation levels described in the previous section. For each selected set of stimulus parameters, the pulse train was modulated at 2 Hz for 10 cycles. The entire experimental stimulation sequence was performed for each implanted electrode.

G. Eye Movement Analysis

Eye movement data were analyzed using a custom software package written in LabVIEW and incorporating 3D rotational kinematics [53]. The calculated SCC axes [based on +x (nasal), +y (left), +z (superior, perpendicular to mean horizontal SCC plane)] were the left-anterior/right-posterior axis (+LARP: $[x,y,z]=[1,-1,0]/\sqrt{2}$), the right-anterior/left-posterior axis (+RALP: $[x,y,z]=[1,1,0]/\sqrt{2}$), and the horizontal axis ($[x,y,z]=[0,0,1]$). For eye responses to sinusoidal stimuli, each of these three components were separately averaged cycle-by-cycle for at least 8 cycles free of saccades and eye blinks. Occasional trials were corrupted due to the animal falling asleep and were disregarded. Several implanted electrodes were too far from their target nerves to elicit significant responses at reasonable current amplitudes and were not included in our study.

Eye rotation velocity in 3D was calculated from eye movement data linearly interpolated on a 1 kHz time base and then filtered by a low pass filter (50-order zero phase finite impulse response filter at 40 Hz) and then a running spline interpolation filter (LabVIEW “Cubic Spline Fit’ module with balance parameter 0.99999). The angle of axis misalignment was computed as the angle between the positive peak (excitatory responses) eye velocity vector (the resultant vector composed of the three eye movement components) and the desired axis of rotation (the axis of the SCC being stimulated). The same calculations were performed for the negative peaks (inhibitory responses).

H. Statistical Analysis

Statistical analysis was performed using the Matlab Statistics and Optimization packages (Mathworks, Natick, MA). Data sets were modeled using either a linear regression (for eye velocity and misalignment vs. SI and IPG) or least-squares fit to a cumulative Gaussian distribution curve (for eye velocity and misalignment vs. current amplitude, charge per phase, and each other), with goodness of fit reported as a correlation coefficient or mean-square error, respectively. Aggregate values are reported as mean ± sample standard deviation (SD).

III. Results

Examples of how spurious stimulation can lead to eye rotation axis misalignment can be seen in Fig. 2. This figure shows eye velocity responses to 10 cycles of 2 Hz modulation of the stimulation (the animals were not physically rotated) delivered to an electrode implanted in the left horizontal SCC of animal CH205 (A) or the left anterior SCC (B), or left posterior SCC of CH207 (C). The stimulus in each case evoked eye rotations mainly about the intended axis; however, the traces corresponding to components of rotation about the other two SCC axes indicate misalignment between the desired and observed axes of eye rotation response. The velocity of the responses were relatively stable over the course of a given 10-cycle trial The peak-to-peak eye response velocities increased 0.74 ± 5.06°/s/cycle (mean ± SD) across all implanted SCCs, which was not significantly different from 0 ($p=0.09$).

Fig. 2 also demonstrates that as for VOR responses to head rotation in individuals with a single normal labyrinth [56,62,63], VOR responses to symmetric sinusoidal gyro inputs in our experiments yielded asymmetric eye movement responses. To quantify this asymmetry, we performed a half-cycle analysis separately considering responses to excitatory and inhibitory half-cycles of stimulation. Across all data sets, the ratio of excitatory response velocity to inhibitory response velocity was 1.30 ± 0.37 (mean ± SD), which is significantly different from the excitatory to inhibitory response ratio of 1.0 in normal animals ($p<0.01$). All data summary figures portray excitatory responses; however, trends reported for response velocity and misalignment as a function of PFM, IPG, PD, and current amplitude were consistent for both inhibitory and excitatory half-cycles across all datasets.

A. Effects of Pulse-Frequency Modulation

For the five SCCs tested across three animals, pulse frequency modulation evoked VOR-mediated eye rotations over a wide dynamic range of velocities while maintaining a nearly constant axis of rotation for all stimuli above SI ~ 20% [Fig. 3], with a nearly linear dependence of peak excitatory VOR response velocity on SI ($R2>0.94$ for all excitatory responses; $R2>0.91$ for all inhibitory responses) in every case [Fig. 3(A)]. The maximum excitatory response velocity observed at SI=100% ranged from 100–400°/s across different SCCs, which is sufficient to encode the majority of head velocities experienced by a chinchilla [59] or human [60] during typical daily activity. The VOR response axis was approximately constant as the SI increased from ~20% to 100%, with a maximum standard deviation of <5° over this range (both excitatory and inhibitory responses) [Fig. 3(B–D)]. Interestingly, misalignment was worse for less intense stimuli: for SI<20% and peak VOR response velocities less than ~50°/s, pulse frequency modulation apparently did not accurately encode the intended axis of head rotation axis [Fig. 3E].

B. Effects of Interphase Gap

For the ten SCCs tested across five animals, varying IPG had no discernible effect on the axis or magnitude of observed evoked eye movements. The effect of varying IPG was studied under two conditions; PD = 180 μs [Fig. 4(A), (C)] and PD = 340 μs [Fig. 4(B), (D)]. For both PD conditions, increasing the IPG from 25–175 μs in steps of 25 μs resulted in no significant changes in either VOR response velocity or axis misalignment. All R2 values were <0.05 for best fit linear regressions for both excitatory and inhibitory responses.

C. Effects of Pulse Duration and Current Amplitude

Eight implanted SCCs were stimulated with pulses that had PD of 340, 270, 180 or 100 μs. Stimulation with shorter PDs requires larger current amplitudes, eventually reaching the limits of the compliance voltage available on the MVP1. Thus, measurable eye movements

were only elicited for 6 of the 8 implanted SCCs with pulses of PD = 50 μs and for 1 of 8 with pulses of PD = 28 μs.

Varying PD had significant effects on the observed VOR eye response movements over a wide range of current amplitudes. Fig. 5 shows observed VOR peak velocities during stimulation of the left horizontal SCC of the same animal described in Fig. 2C. For stimulation with each PD, VOR response velocity increased with increasing current amplitude [Fig. 5(A)] and with increasing charge per phase [Fig. 5(B)]. Stimulation with shorter PD required less charge per phase to elicit a given VOR response velocity [Fig. 5(B)]. Not surprisingly, VOR response axis misalignment also increased with increasing current amplitude [Fig. 5(C)] and increasing charge per phase [Fig. 5(D)] for each PD employed. These trends were consistent for all SCCs tested.

For any given VOR response velocity, stimulation with PD = 50 and 100 μs evoked responses with the smallest misalignments while longer PDs evoked larger misalignments [Fig. 5(E)]. This trend was especially apparent for lower-current stimuli, but was consistent across the range of responses observed in seven of the eight tested SCCs. (One dataset showed decreased misalignment with increased current amplitude and charge per phase.) For example, Fig. 6 shows the axis of VOR responses elicited by stimulation of the left horizontal SCC of chinchilla CH205 using PD ranging from 50 μs to 340 μs with current amplitude adjusted in each case to elicit a peak eye rotation velocity of 200°/s (which was half of the maximum observed eye velocity for this SCC). Misalignment increased monotonically with increasing PD, from 19° at 50 μs to 36° at 340 μs.

This trend of increasing misalignment with increasing PD for a given velocity was observed across all analyzed SCCs to have an increasing slope of 0.03 ± 0.025°/μs (mean ± SD) for excitatory responses and 0.027 ± 0.023°/μs for inhibitory responses [Fig. 7(A)]. The mean slopes were significantly different from 0 ($p=0.01$ for both). Changes in PD had a more pronounced effect (a steeper slope of a regression line fit to a misalignment vs. PD plot) for SCC datasets that had responses with large misalignment even under their best conditions. As Fig. 7B shows, this relationship is statistically significant: when the slopes of regression fits in Fig. 7A are plotted versus the misalignment observed at a low PD (100 μs), the best fit linear regression line to the resulting data has positive slope and $R2 = 0.81$. These results show that an electrode eliciting highly selective stimulation and low misalignment (probably because it was fortuitously implanted very close to its target ampullary nerve) maintains low misalignment over a wide range of PD, while the responses for an electrode that is less selectively coupled to its ampullary nerve target can be optimized by using the shortest PD achievable.

Four of the implanted SCCs were stimulated relative to a “near” reference electrode and the other four were stimulated relative to a “distant” reference electrode (Table 1). This study was not designed to systematically study effects of near vs. far return electrodes, so only a single reference arrangement was used for each case. No significant effect was observed for “near” vs. “far” reference conditions for the 8 animal/SCC combinations studied ($p>0.2$ for all conditions). It is important to note that lack of finding a significant difference between two N=4 subgroups in a post-hoc statistical analysis for which the study was not designed does not constitute adequate support to draw a strong inference regarding whether “near” and “far” references would yield significantly different results in a large sample population.

IV. Discussion

The goal of this study is to provide guidance for the design of a vestibular prosthesis stimulus protocol that can effectively restore head motion sensation to individuals disabled

by bilateral loss of vestibular function. While quantitative differences in optimal parameters between chinchillas and humans are likely, the relative importance of different stimulus parameters is probably conserved across species. We therefore sought to identify a key subset of stimulus features that can allow encoding of head velocity (i.e., gyro inputs) over a wide dynamic range with minimal misalignment.

A. Pulse-Frequency Modulation (PFM) as the Basic Code

Ideally, a vestibular prosthesis intended to restore SCC function should engender vestibular nerve activity that accurately encodes head rotations in 3 dimensions over the full range of speeds and directions encountered in typical daily activities. Consistent with prior studies [18,23], we confirmed that PFM is an appropriate basis for a stimulation strategy because it elicited VOR responses over a wide dynamic range of velocities (as high as 400°/s peak) with a relatively constant axis of rotation for SIs between ~20% and 100% (Fig. 3). While modulating other stimulus features might enhance or fine tune responses, we conclude that pulse-frequency modulation by head velocity should be the fundamental coding paradigm. This is a departure from the standard approach used in cochlear implants, which generally involves an amplitude-modulation scheme (e.g., continuous interleaved sampling). Employing such a strategy in the vestibular prosthesis would likely lead to undesirable variations in misalignment as the current is modulated [Fig. 5(C)].

Observed VOR axis misalignment was larger for SI less than ~20%. For the smallest responses elicited at very low SI, the apparent increase in misalignment may have been due to difficulty in accurately measuring the axis of rotation. However, the increased misalignment was apparent even when responses were well above our eye movement measurement system's velocity noise floor (3°/s RMS, 5°/s peak in each dimension) [53], and we have observed similar effects in recent experiments using scleral search coils in rhesus monkeys [61]. It should be noted that when the axis of eye rotation was misaligned with the intended axis of rotation, it always shifted toward one or both of the other two (non-target) SCC axes [Fig. 3(C)]. This supports the interpretation that misalignment is caused by current spread to the non-target SCCs' ampullary nerves. Furthermore, it is likely that posterior SCC stimulation generally elicited the lowest misalignment because its nerve is located relatively far from the other two SCCs' nerves.

Even though the PFM was quasi-sinusoidal in shape, some inhibitory responses exhibited non-sinusoidal characteristics (e.g., inflection point part-way through inhibitory half-cycle) that did not become more sinusoidal over time [Fig. 2(C)]. This may have been due to the implementation of a piecewise-linear velocity-to-pulse-rate mapping [Fig. 1(B)] as opposed to a continuous, sigmoidal mapping, which did not elicit this effect [18, 23].

Without performing single-unit recordings from vestibular afferents or interneurons, we cannot know exactly how our pulsatile stimuli interact with spontaneous activity on afferent fibers. However, some reasonable hypotheses can be drawn from available evidence [47,64]. For low stimulus pulse rates and pulse amplitudes well above threshold, total spike rate is probably close to a simple sum of exogenous and spontaneous rates, so down-modulation of prosthetic input to zero probably cannot reduce actual spike rates below the innate spontaneous activity (which after intratympanic gentamicin is typically about half of pre-injury spontaneous rates) [56,65]. A saturating nonlinearity probably occurs for high exogenous pulse rates (e.g., when the inter-pulse interval is much shorter than the spontaneous inter-spike interval), so up-modulation of prosthetic input to more than twice the innate spontaneous rate probably results in synchronized firing of all super-threshold regular afferents at the exogenous pulse rate, while the faster after-hyperpolarization potential recovery of irregular afferents might result in a persistent contribution of innate, irregular spontaneous activity that becomes relatively small as exogenous rates rise.

B. Short Pulse Duration Requires Less Power and Elicits Less Misalignment

Pulses with shorter PD required less charge per phase to elicit equivalent given peak VOR velocity response than did longer PD pulses. This observation is in agreement with classical strength-duration characteristics described for electrical stimulation studies in other sensory modalities, as initially posed by Lapicque [40,41], significantly refined by Hill [39], and recently reviewed by Merrill *et al.* [32]. As shown in Fig. 8, the current amplitude required to elicit a given peak VOR response velocity depends on PD according to a logistic type function similar to that Grill and Mortimer [29] adapted from Lapicque's original description:

$$I=K/(1-e^{-PD/\tau}) \quad (1)$$

where K = a rheobase current (equal to 98, 119, 137, 163 μA/phase for peak velocity of 50, 80, 120, 150 °/s, respectively) and τ is a time constant (118 μs; all values were obtained through a least-squares fit constrained to uniform τ.) Using shorter PD stimuli requires passage of less charge and encounters lower electrode impedance (because metal-saline interfaces are dominated by capacitive reactance for our stimuli). Therefore, using shorter PD should require less power (as long as the compliance voltage required to achieve higher currents is available) and could conserve battery life of a head-mounted device. Pulses with shorter PD and lower charge per phase are also less likely to generate corrosive electrochemistry byproducts [32]. Finally, shorter PD's also yield a benefit in that they allow higher pulse rates and nonoverlapped interleaving of stimuli on a larger number of electrodes.

The fact that stimulation with pulses of shorter PD resulted in a decreased VOR response axis misalignment for a given VOR response velocity suggests that shorter PD results in more spatially selective excitation of the targeted ampullary nerve. This effect is consistent with electrical stimulation studies in the sciatic nerve [66], auditory nerve [43], and retinal ganglion cells [31]. A neuromorphic model proposing a biophysical basis for this phenomenon has been described by Grill and Mortimer [29].

In two of the eight implanted SCCs, changes in PD did not significantly change the VOR response axis (Fig. 7(A), CH207LA and CH207LH). In both of these cases, the misalignment was less than 13° for all PD values tested. This probably indicates fortuitous surgical placement of the stimulating electrodes very close to their target ampullary nerves, resulting in little spurious stimulation of neighboring nerve branches. While such accurate placement is always a goal, it cannot always be realized. As shown by the data in Fig. 7, cases in which spurious stimulation is problematic (probably electrodes positioned almost equidistant between target and non-target nerve fibers) benefit the most from shifting to the shortest PD possible.

C. IPG Has No Effect Over the Range Tested

Variation of IPG had essentially no effect on VOR response velocity or axis over the range of IPGs tested (25–175 μs). This observation is consistent with analogous studies conducted on cochlear implants over a similar range of IPGs, which reported that as the IPG of the stimulation waveform was increased from 45 to 100 μs, current amplitude required to maintain perception of equal loudness increased by only 0.3 dB [45,46]. A minimal effect of IPG on misalignment was also consistent with a psychophysical study conducted in cochlear implant patients by van Wieringen *et al.*, who found that varying the IPG in cochlear implants did not significantly influence the spatial selectivity of the stimulation pulses [51]. We suspect that an IPG of 0 μs would result in higher thresholds than we observed at IPG of

25 μs; however, this was not explored because the control code of the prosthesis used for this study required a minimum IPG of 25 μs.

D. Complements to Optimization of Stimulus Timing

While our focus in this study has been on optimization of stimulus timing, performance of multichannel vestibular prostheses will likely be improved along multiple lines of development. Several techniques have been proposed to simultaneously enhance dynamic range and decrease misalignment of prosthetic vestibular stimulation: (1) Improvements in electrode design and surgical technique can help place stimulating electrodes in closer vicinity to target nerve branches, thereby increasing an electrode's coupling with the target nerve and better isolating it from non-target nerve branches (e.g., [67,68]). (2) Multipolar electrode paradigms can "steer" stimulus current toward target nerve branches and away from others [69]. (3) Orthogonalizing the coordinate system using linear algebra techniques can partly correct for misalignment due to current spread by specifying the correct combination of stimulus intensity on each of 3 SCC electrodes to engender the desired response through vector superposition [14,21]. (4) Rehabilitation exercises designed to augment and better align gaze stabilizing reflexes through central adaptive mechanisms can improve overall gaze stability despite the distorted vestibular nerve activity engendered by prosthetic stimulation [15,16,70,71]. (5) Exploiting differential sensitivity of regular and irregular vestibular afferent fibers to electrical stimuli might present the central nervous system with a pattern of neural activity that more closely recreates the firing patterns generated by a normal inner ear [64,72].

In light of experience with optimization of cochlear implant performance [26], restoration of stable gaze and posture in individuals disabled by loss of vestibular sensation will likely require some combination of several of these approaches. While specific values reported herein depend on microanatomy, electrode location and degree of neural survival in each case, qualitative aspects of these findings will likely hold true across species, including humans.

Acknowledgments

Supported by NIH NIDCD grants: R01DC009255, 1F31DC010099-01A1.

References

1. Carey, JP.; Della Santina, CC. Principles of applied vestibular physiology. In: Cummings, CW., editor. Otolaryngology - Head & Neck Surgery. Elsevier; 2005. p. 3115-3159.
2. Black FO, Gianna-Poulin C, Pesznecker SC. Recovery from vestibular ototoxicity. Otology & Neurotology. 2001; 22:662–671. [PubMed: 11568676]
3. Black FO, Pesznecker S, Stallings V. Permanent gentamicin vestibulotoxicity. Otology & Neurotology. 2004; 25:559–569. [PubMed: 15241236]
4. Mamoto Y, Yamamoto K, Imai T, Tamura M, Kubo T. Three-dimensional analysis of human locomotion in normal subjects and patients with vestibular deficiency. Acta Oto-Laryngologica. 2002; 122:495–500. [PubMed: 12206257]
5. Rinne T, Bronstein AM, Rudge P, Gresty MA, Luxon LM. Bilateral loss of vestibular function: clinical findings in 53 patients. Journal of Neurology. 1998; 245:314–321. [PubMed: 9669481]
6. Minor LB. Gentamicin-induced bilateral vestibular hypofunction. Jama-Journal of the American Medical Association. 1998; 279:541–544.
7. Della Santina CC, Potyagaylo V, Migliaccio AA, Minor LB, Carey JP. Orientation of human semicircular canals measured by three-dimensional multiplanar CT reconstruction. Jaro-Journal of the Association for Research in Otolaryngology. 2005; 6:191–206.

8. Ewald, JR. Physiologische untersuchugen uber das Endorgans des Nervus Octavus: Bergmann. 1892.
9. Wilson, VJ.; Melvill, J. Mammalian vestibular physiology. New York: Plenum; 1979.
10. Cohen B, Suzuki J, Bender MB. Eye Movements from Semicircular Canal Nerve Stimulation in Cat. Annals of Otology Rhinology and Laryngology. 1964; 73:153.
11. Suzuki J, Cohen B, Bender MB. Compensatory Eye Movements Induced by Vertical Semicircular Canal Stimulation. Experimental Neurology. 1964; 9:137. [PubMed: 14126123]
12. Suzuki JI, Cohen B. Head Eye Body + Limb Movements from Semicircular Canal Nerves. Experimental Neurology. 1964; 10:393. [PubMed: 14228399]
13. Suzuki JI, Goto K, Tokumasu K, Cohen B. Implantation of Electrodes near Individual Vestibular Nerve Branches in Mammals. Annals of Otology Rhinology and Laryngology. 1969; 78:815.
14. Merfeld DM, Haburcakova C, Gong W, Lewis RF. Chronic vestibulo-ocular reflexes evoked by a vestibular prosthesis. IEEE Transactions on Biomedical Engineering. 2007; 54:1005–1015. [PubMed: 17554820]
15. Merfeld DM, Gong WS, Morrissey J, Saginaw M, Haburcakova C, Lewis RF. Acclimation to chronic constant-rate peripheral stimulation provided by a vestibular prosthesis. IEEE Transactions on Biomedical Engineering. 2006; 53:2362–2372. [PubMed: 17073343]
16. Lewis RF, Gong WS, Ramsey M, Minor L, Boyle R, Merfeld DM. Vestibular adaptation studied with a prosthetic semicircular canal. Journal of Vestibular Research-Equilibrium & Orientation. 2002; 12:87–94.
17. Gong WS, Merfeld DM. System design and performance of a unilateral horizontal semicircular canal prosthesis. IEEE Transactions on Biomedical Engineering. 2002; 49:175–181. [PubMed: 12066886]
18. Gong WS, Merfeld DM. Prototype neural semicircular canal prosthesis using patterned electrical stimulation. Annals of Biomedical Engineering. 2000; 28:572–581. [PubMed: 10925955]
19. Lewis RF, Merfeld DM, Gong WS. Cross-axis vestibular adaptation produced by patterned electrical stimulation. Neurology. 2001; 56:A18–A18.
20. Gong WS, Haburcakova C, Merfeld DM. Vestibulo-Ocular Responses Evoked Via Bilateral Electrical Stimulation of the Lateral Semicircular Canals. IEEE Transactions on Biomedical Engineering. 2008; 55:2608–2619. [PubMed: 18990631]
21. Fridman GY, Davidovics N, Dai C, Della Santina CC. Multichannel Vestibular Prosthesis Stabilizes Eyes For Head Rotation About Any Axis. Journal of the Association for Research in Otolaryngology. 2009 vol. Submitted 2009.
22. Chiang, B.; Fridman, GY.; Della Santina, CC. Enhancements to the Johns Hopkins Multi-Channel Vestibular Prosthesis Yield Reduced Size, Extended Battery Life, Current Steering and Wireless Control. presented at Association for Research in Otolaryngology Abst. 867; Baltimore, MD. 2009.
23. Della Santina CC, Migliaccio AA, Patel AH. A multichannel semicircular canal neural prosthesis using electrical stimulation to restore 3-D vestibular sensation. IEEE Transactions on Biomedical Engineering. 2007; 54:1016–1030. [PubMed: 17554821]
24. Della Santina C, Migliaccio A, Patel A. Electrical stimulation to restore vestibular function development of a 3-d vestibular prosthesis. Conf Proc IEEE Eng Med Biol Soc. 2005; 7:7380–5. [PubMed: 17281986]
25. Grossman GE, Leigh RJ, Bruce EN, Huebner WP, Lanska DJ. Performance of the Human Vestibuloocular Reflex During Locomotion. Journal of Neurophysiology. 1989; 62:264–272. [PubMed: 2754477]
26. Wilson BS, Dorman MF. Cochlear implants: A remarkable past and a brilliant future. Hearing Research. 2008; 242:3–21. [PubMed: 18616994]
27. Wilson BS, Finley CC, Lawson DT, Wolford RD, Eddington DK, Rabinowitz WM. Better speech recognition with cochlear implants. Nature. 1991; 352:236–238. [PubMed: 1857418]
28. Zeng, FG.; Popper, AN.; Fay, RR. Cochlear Implants: Auditory Prostheses and Electric Hearing. New York: Springer-Verlag; 2004.
29. Grill WM, Mortimer JT. The effect of stimulus pulse duration on selectivity of neural stimulation. IEEE Transactions on Biomedical Engineering. 1996; 43:161–166. [PubMed: 8682527]

30. Gorman PH, Mortimer JT. The Effect of Stimulus Parameters on the Recruitment Characteristics of Direct Nerve-Stimulation. IEEE Transactions on Biomedical Engineering. 1983; 30:407–414. [PubMed: 6604691]

31. Ahuja AK, Behrend MR, Kuroda M, Humayun MS, Weiland JD. An in vitro model of a retinal prosthesis. IEEE Transactions on Biomedical Engineering. 2008; 55:1744–1753. [PubMed: 18714839]

32. Merrill DR, Bikson M, Jefferys JGR. Electrical stimulation of excitable tissue: design of efficacious and safe protocols. Journal of Neuroscience Methods. 2005; 141:171–198. [PubMed: 15661300]

33. Baird RA, Desmadryl G, Fernandez C, Goldberg JM. The Vestibular Nerve of the Chinchilla .2. Relation between Afferent Response Properties and Peripheral Innervation Patterns in the Semicircular Canals. Journal of Neurophysiology. 1988; 60:182–203. [PubMed: 3404216]

34. Fernandez C, Baird RA, Goldberg JM. The Vestibular Nerve of the Chinchilla .1. Peripheral Innervation Patterns in the Horizontal and Superior Semicircular Canals. Journal of Neurophysiology. 1988; 60:167–181. [PubMed: 3404215]

35. Hullar TE, Minor LB. High-frequency dynamics of regularly discharging canal afferents provide a linear signal for angular vestibuloocular reflexes. J Neurophysiol. 1999; 82:2000–5. [PubMed: 10515990]

36. Lewis RF, Haburcakova C, Merfeld DM. Roll tilt psychophysics in rhesus monkeys during vestibular and visual stimulation. Journal of Neurophysiology. 2008; 100:140–153. [PubMed: 18417632]

37. Della Santina, CC.; Migliaccio, AA.; Patel, AH. Electrical stimulation to restore vestibular function - development of a 3-D vestibular prosthesis. presented at 27th Annual IEEE Engineering in Medicine and Biology; Shanghai, China. 2005.

38. Prado-Guitierrez P, Fewster LM, Heasman JM, McKay CM, Shepherd RK. Effect of interphase gap and pulse duration on electrically evoked potentials is correlated with auditory nerve survival. Hearing Research. 2006; 215:47–55. [PubMed: 16644157]

39. Hill AV. Excitation and accomodation in nerve. Proc R Soc B. 1936; 119:305–355.

40. Lapicque L. Recherches quantitatives sur l'excitation électrique des nerfs traitée comme une polarisation. Journal de Physiologie et de Pathologie Générale. 1907; 9:620–635.

41. Lapicque L. Quantitative investigations of electrical nerve excitation treated as polarization. 1907. Biol Cybern. 2007; 97:341–9. [PubMed: 18046573]

42. Vandenhonert C, Stypulkowski PH. Physiological-Properties of the Electrically Stimulated Auditory-Nerve .2. Single Fiber Recordings. Hearing Research. 1984; 14:225–243. [PubMed: 6480511]

43. McKay CM, McDermott HJ. The perceptual effects of current pulse duration in electrical stimulation of the auditory nerve. Journal of the Acoustical Society of America. 1999; 106:998–1009. [PubMed: 10462805]

44. Warman EN, Grill WM, Durand D. Modeling the Effects of Electric-Fields on Nerve-Fibers - Determination of Excitation Thresholds. IEEE Transactions on Biomedical Engineering. 1992; 39:1244–1254. [PubMed: 1487287]

45. Carlyon RP, van Wieringen A, Deeks JM, Long CJ, Lyzenga J, Wouters J. Effect of inter-phase gap on the sensitivity of cochlear implant users to electrical stimulation. Hearing Research. 2005; 205:210–224. [PubMed: 15953530]

46. McKay CM, Henshall KR. The perceptual effects of interphase gap duration in cochlear implant stimulation. Hearing Research. 2003; 181:94–99. [PubMed: 12855367]

47. Shepherd RK, Javel E. Electrical stimulation of the auditory nerve: II. Effect of stimulus waveshape on single fibre response properties. Hearing Research. 1999; 130:171–188. [PubMed: 10320107]

48. Vandenhonert C, Mortimer JT. Response of the Myelinated Nerve-Fiber to Short Duration Biphasic Stimulating Currents. Annals of Biomedical Engineering. 1979; 7:117–125. [PubMed: 533020]

49. van Wieringen A, Carlyon RP, Macherey O, Wouters J. Effects of pulse rate on thresholds and loudness of biphasic and alternating monophasic pulse trains in electrical hearing. Hearing Research. 2006; 220:49–60. [PubMed: 16904278]
50. van Wieringen A, Macherey O, Carlyon RP, Deeks JM, Wouters J. Alternative pulse shapes in electrical hearing. Hear Res. 2008; 242:154–63. [PubMed: 18468821]
51. van Wieringen, A.; Carlyon, RP.; Wouters, J. Spatial excitation patterns of different pulse shapes and electrode configurations in cochlear implantees. presented at Conference on Implantable Auditory Prostheses; Asilomar, CA, USA. 2005.
52. Tang S, Melvin TAN, Della Santina CC. Effects of semicircular canal electrode implantation on hearing in chinchillas. Acta Oto-Laryngologica. 2009; 129:481–486. [PubMed: 18615331]
53. Migliaccio AA, MacDougall HG, Minor LB, Della Santina CC. Inexpensive system for real-time 3-dimensional video-oculography using a fluorescent marker array. Journal of Neuroscience Methods. 2005; 143:141–150. [PubMed: 15814146]
54. Hullar TE, Della Santina CC, Hirvonen T, Lasker DM, Carey JP, Minor LB. Responses of irregularly discharging chinchilla semicircular canal vestibular-nerve afferents during high-frequency head rotations. Journal of Neurophysiology. 2005; 93:2777–2786. [PubMed: 15601735]
55. Davidovics, N.; Fridman, GY.; Della Santina, CC. Linearity of Stimulus-Response Mapping During Semicircular Canal Stimulation using a Vestibular Prosthesis. presented at Association for Research in Otolaryngology Abst. 339; Baltimore. 2009.
56. Hirvonen TP, Minor LB, Hullar TE, Carey JP. Effects of intratympanic gentamicin on vestibular afferents and hair cells in the chinchilla. Journal of Neurophysiology. 2005; 93:643–655. [PubMed: 15456806]
57. Migliaccio, AA.; Minor, L.; Della Santina, CC. The 3-Dimensional Angular Vestibulo-Ocular Reflex Evoked by High-Acceleration Rotations in Normal Chinchilla Is Conjugate, Nonlinear and Isotropic. presented at Association for Research in Otolaryngology; Denver, CA. 2007.
58. Hullar TE, Williams CD. Geometry of the semicircular canals of the chinchilla (Chinchilla laniger). Hearing Research. 2006; 213:17–24. [PubMed: 16439079]
59. Hayden, R. Biomedical Engineering. Baltimore: Johns Hopkins; 2007. A model to guide electrode design for a multichannel vestibular prosthesis; p. 139vol. MS
60. Grossman GE, Leigh RJ, Abel LA, Lanska DJ, Thurston SE. Frequency and Velocity of Rotational Head Perturbations During Locomotion. Experimental Brain Research. 1988; 70:470–476.
61. Dai, C.; Fridman, GY.; Della Santina, C. Effects of Vestibular Electrode Implantation and Prosthetic Stimulation on Hearing in Rhesus Monkeys. presented at Association for Research in Otolaryngology; Orange County, CA. 2010.
62. Halmagyi GM, Aw ST, Cremer PD, Todd MJ, Curthoys IS. The Human Vertical Vestibuloocular Reflex in Response to High-Acceleration Stimulation after Unilateral Vestibular Neurectomy. Annals of the New York Academy of Sciences. 1992; 656:732–738. [PubMed: 1599178]
63. Sadeghi SG, Minor LB, Cullen KE. Response of vestibular-nerve afferents to active and passive rotations under normal conditions and after unilateral labyrinthectomy. Journal of Neurophysiology. 2007; 97:1503–1514. [PubMed: 17122313]
64. Goldberg JM, Smith CE, Fernandez C. Relation between Discharge Regularity and Responses to Externally Applied Galvanic Currents in Vestibular Nerve Afferents of the Squirrel-Monkey. Journal of Neurophysiology. 1984; 51:1236–1256. [PubMed: 6737029]
65. Della Santina, CC.; Migliaccio, AA.; Park, HJ.; Anderson, ICW.; Jiradejvong, P.; Minor, LB.; Carey, JP. 3D Vestibuloocular reflex, afferent responses and crista histology in chinchillas after unilateral intratympanic gentamicin. presented at Association for Research in Otolaryngology Annual Mtg; New Orleans. 2005.
66. Grill WM, Mortimer JT. Neural and connective tissue response to long-term implantation of multiple contact nerve cuff electrodes. Journal of Biomedical Materials Research. 2000; 50:215–226. [PubMed: 10679687]
67. Gstoettner WK, Adunka O, Franz P, Hamzavi J, Plenk H, Susani M, Baumgartner W, Kiefer J. Perimodiolar electrodes in cochlear implant surgery. Acta Oto-Laryngologica. 2001; 121:216–219. [PubMed: 11349782]

68. Middlebrooks JC, Snyder RL. Auditory prosthesis with a penetrating nerve array. Jaro-Journal of the Association for Research in Otolaryngology. 2007; 8:258–279.

69. Bonham BH, Litvak LM. Current focusing and steering: Modeling, physiology, and psychophysics. Hearing Research. 2008; 242:141–153. [PubMed: 18501539]

70. Scherer M, Migliaccio AA, Schubert MC. Effect of vestibular rehabilitation on passive dynamic visual acuity. Journal of Vestibular Research-Equilibrium & Orientation. 2008; 18:147–157.

71. Schubert MC, Della Santina CC, Shelhamer M. Incremental angular vestibulo-ocular reflex adaptation to active head rotation. Experimental Brain Research. 2008; 191:435–446.

72. Goldberg JM. Afferent diversity and the organization of central vestibular pathways. Experimental Brain Research. 2000; 130:277–297.

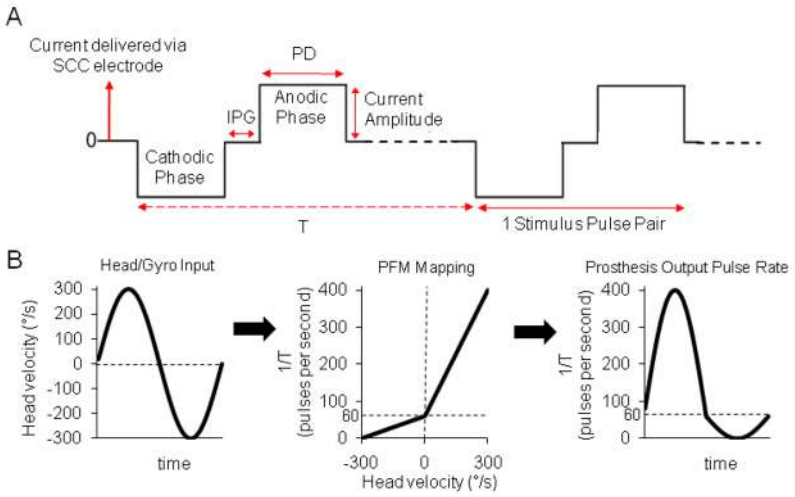

Fig. 1.

(A) Three parameters define a cathodic-first, symmetric, biphasic, electrical stimulation pulse: current amplitude, pulse duration (PD), and interphase gap (IPG). T = time interval between pulse pairs. (B) The stimulus encoding scheme used for each of three dimensions of head rotation converts head velocity about a given semicircular canal axis to modulation of pulse rate f = 1/T on the corresponding electrodes via a piecewise-linear velocity-to-pulse rate mapping meant to efficiently approximate the mean operating characteristic of vestibular nerve afferent fibers. Stimulus intensity = 100% is depicted here.

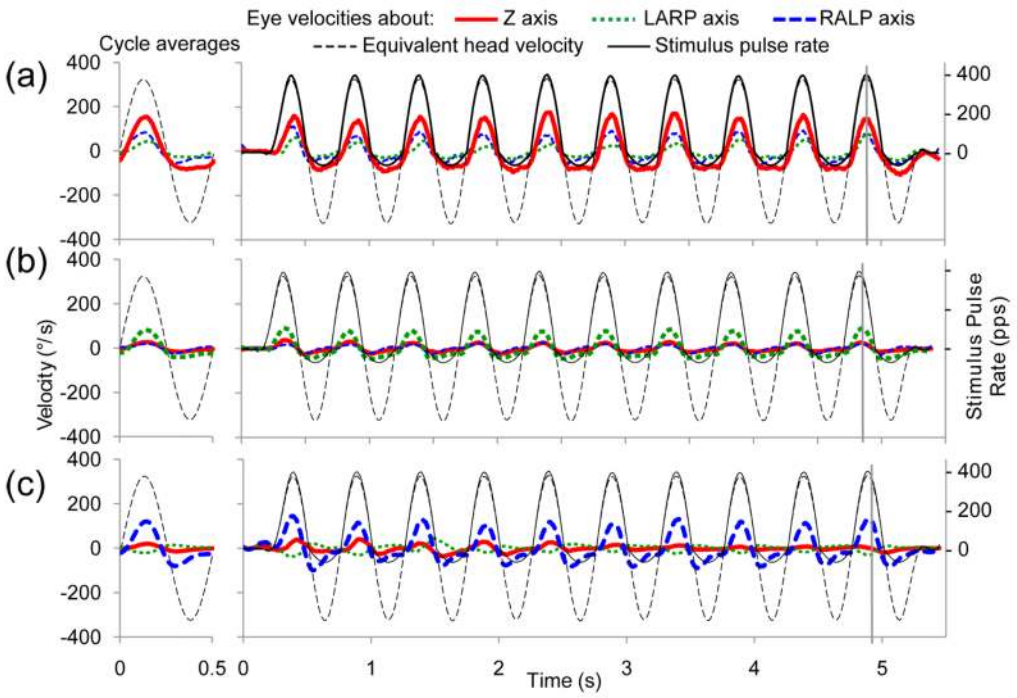

Fig. 2.

Eye velocity responses to pulse-frequency-modulated, constant current, symmetric biphasic pulses delivered at a modulation frequency of 2 Hz with stimulus intensity = 100% to the left horizontal semicircular (SCC) of CH205 (A), the left anterior SCC of CH207 (B), and the left posterior SCC of CH207 (C). Thick red/solid line indicates the component of eye movement about the horizontal axis, green/dotted line indicates the left anterior-right posterior (LARP) axis, and blue/dashed line indicates the right-anterior/left-posterior (RALP) axis. Thin black/dashed trace shows the angular head velocity about the RALP axis equivalent to the stimulus presented. Thin black/solid trace represents the delivered pulse rate of the stimulus (right-hand ordinate). Vertical gray lines represent the time of peak eye velocity for a given cycle. Mean responses for each dataset are in the left column (SD<19 dps for all datasets). The animal was kept stationary to examine responses to electrical stimulation alone. The largest amplitude trace in each figure represents the eye movement component about the desired axis of rotation while other traces represent undesired eye movement components. Refer to Fig. 3D for orientation of eye movement axes.

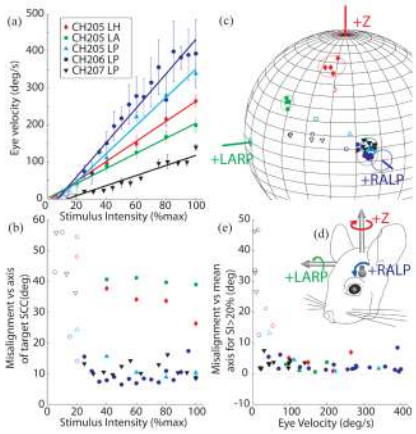

Fig. 3.

Peak excitatory response eye velocity (A) and misalignment (B) as a function of stimulus intensity for 5 implanted SCCs. In each case, pulse frequency modulation (PFM) of biphasic current pulses was used to encode a virtual sinusoidal head velocity at 2 Hz as described in text. Stimulus intensity (SI) of 100% corresponds to PFM about a baseline of 60 pps up to 400 pps and down to 0 pps. SI<100% implies a proportional decrease in pulse rate excursion about the baseline. In all cases, VOR response eye velocity increased almost linearly with increasing SI (R2>0.94 for each case), while misalignment between the desired and observed VOR axes remained relatively constant for SI>20%. (C) Axes of responses for each SCC tested cluster tightly in each case about a constant axis for SI>20% (solid symbols) but depart from that axis for lower SI (open symbols). Circles around the data points represent 3 standard deviations of misalignment angle beyond the mean axis of responses for SI>20%. Angle measurement error for each SCC axis (depicted in (D) in reference to an animal head) is based on animal measurements [58]. (E) To more clearly depict the consistency of the misalignment across eye response velocities, misalignment with respect to mean response axes to stimuli with SI>20% for each SCC is plotted against eye velocity. Axis of rotation remains relatively constant for peak excitatory eye responses>50°/s.

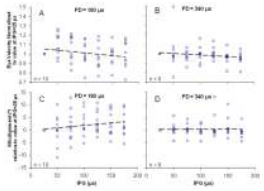

Fig. 4.

Effect of variation in interphase gap (IPG). Symmetric biphasic pulses with varying IPG were delivered to 10 implanted SCCs in 5 animals at two different pulse durations (PD), 180 μs and 340 μs. The current amplitude was halfway between threshold and maximum current levels. For the range of IPGs tested, no significant effect was observed on either the VOR response eye velocity (A,B) or axis misalignment (C,D). $R2 < 0.05$ for regression lines in all panels.

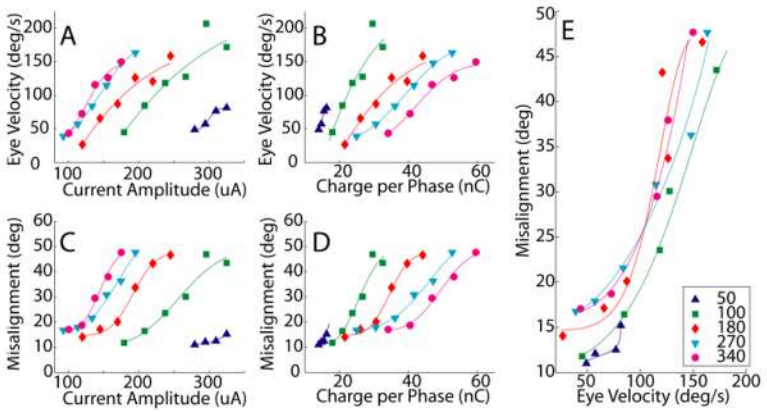

Fig. 5.

Stimulation pulses with varying pulse durations (PD) were delivered to the left horizontal SCC of animal CH207 at a range of current amplitudes. Peak excitatory response eye velocity increased with increasing current (A) and charge per phase (B) for all PD tested. Misalignment also increased with increasing current (C) and charge per phase (D) for all PD tested. Shorter PD stimuli required less charge per phase to evoke eye responses of a given velocity (B) and achieved a given velocity with less change in eye movement axis (E) than did longer PD stimuli. Changes in current (or charge) can encode changes in head velocity below ~75°/s without changing axis, but eye rotation axis shifts dramatically as current is increased to encode higher eye velocities. Curves in A–D are least-mean-square fits of cumulative Gaussian distribution functions; curves in E were derived from those fit to A and C.

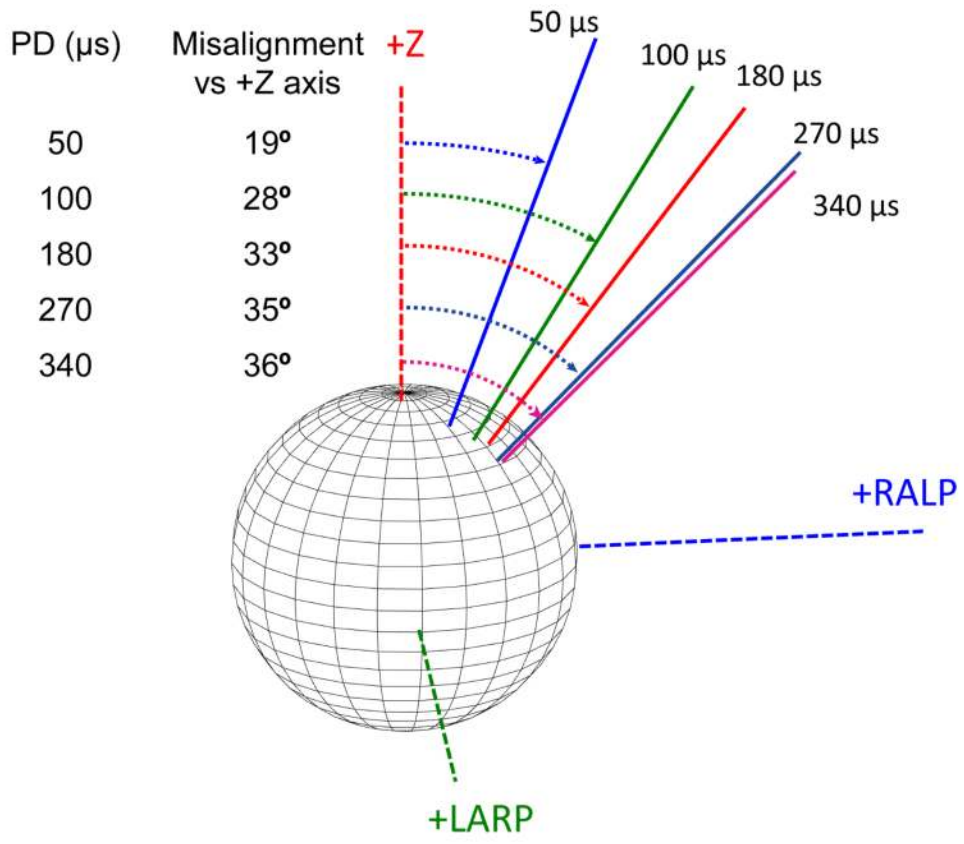

Fig. 6.
Longer PD pulses result in responses with greater misalignment versus the desired horizontal axis eye rotation for a given eye velocity of 200°/s (CH205, left horizontal SCC electrode).

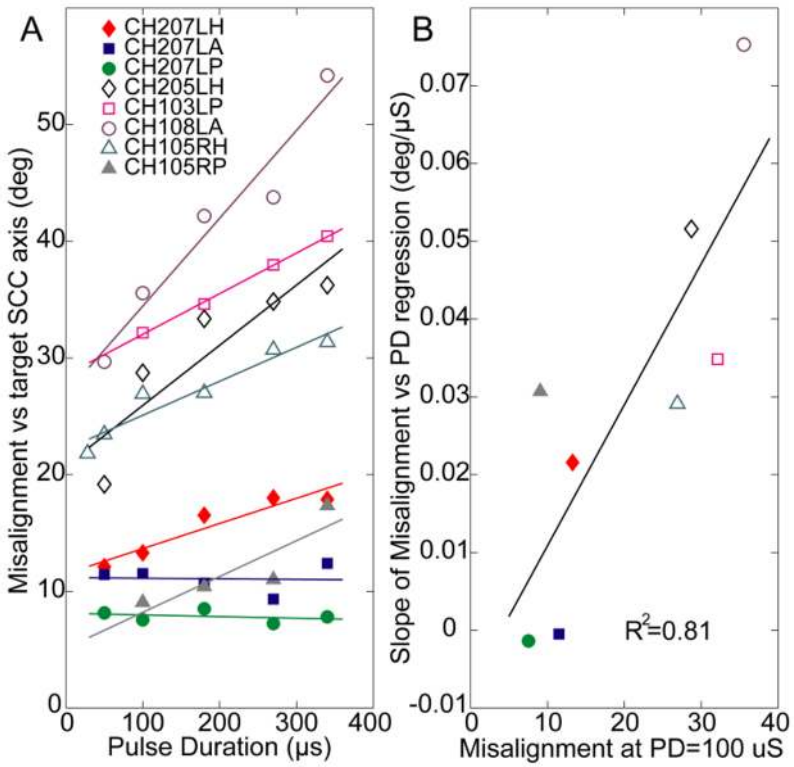

Fig. 7.

(A) Misalignment increased with increasing PD for 6 of the 8 SCCs tested; current amplitude chosen in each case to yield half-maximal eye velocity). (B) Cases with the worst (highest) misalignment measured at PD = 100 μs have the greatest potential for improvement with shorter PD (R2 = 0.81).

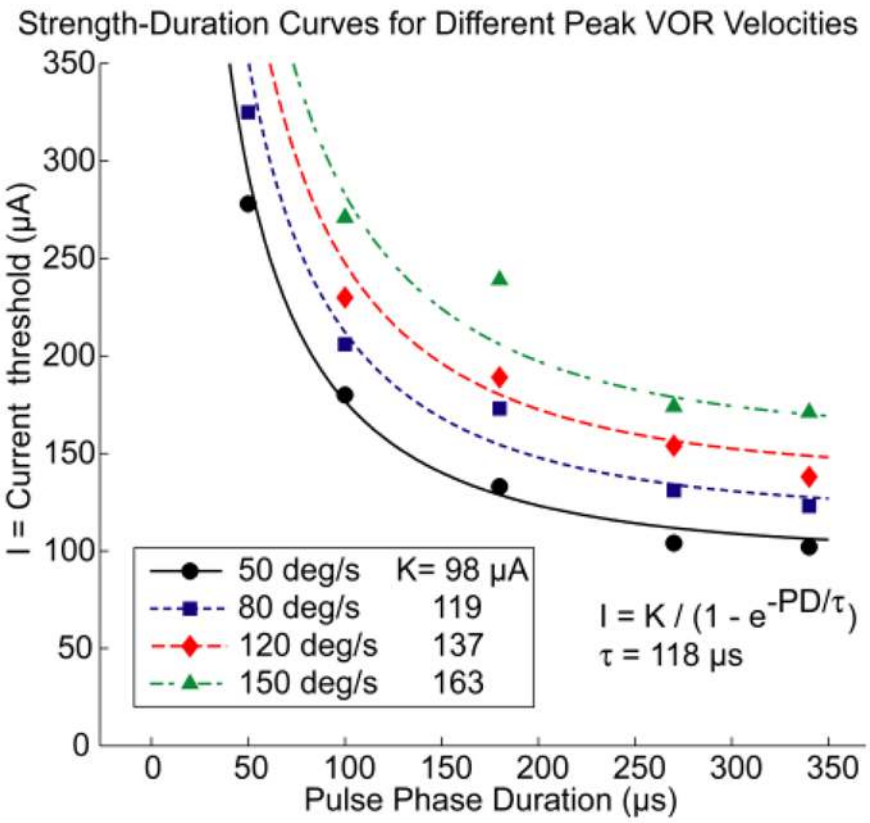

Fig. 8.

The relationship between PD and current required to elicit eye rotation at a specified peak excitatory response velocity is well described by a family of classic strength-duration curves with time constant 118 μs. [29,40,41]

Table 1

Maximal eye velocity, current at maximum velocity, misalignment, and reference electrode arrangement for each case. Responses to stimulation using “near” and “distant” reference electrodes demonstrate no clear effect observed due to reference electrode type. Misalignment values are at half-maximal eye velocities. Stimulus intensity = 100%, PD = 100 μs. Numbers in left column denote animals.

Implanted canal	Max eye velocity (°/s)	Current at max eye velocity (μA)	Misalignment (°)	Reference electrode
205 LH	250	230	28	Near
207 LH	205	295	13	Near
207 LA	395	250	12	Near
207 LP	500	220	8	Near
103 LP	230	325	32	Distant
105 RH	235	150	27	Distant
105 RP	305	300	9	Distant
108 LA	75	155	36	Distant